



FENTON, PHOTO AND PHOTO-FENTON DEGRADATION PERFORMANCE OF Fe₃O₄/g-C₃N₄ NANOCOMPOSITE ON RhB DYE AND THEIR CHARACTERIZATION STUDIES

Arjun Moorthy¹, S. Satheeskumar^{2*}, S. Surendhiran³, R. Mohanraj⁴, B. Kalpana⁵, K.S. Balu⁶

Abstract

The Fenton process is one of the most prominent advanced oxidation techniques for the treatment of wastewater in industrial effluents. Also, the traditional homogeneous Fenton process possesses a few limitations, such as sludge formation, and addition of catalyst for every batch of treatment. To address these heterogeneous recyclable Fenton processes, Fe₃O₄/g-C₃N₄ nanocomposites have been developed. The Fe₃O₄ nanoparticles here have been prepared by a simple sol-gel technique with a single ion precursor. The nanoparticles formed were polycrystalline and determined the particles to be nearly 30 nm in size. The purity and crystalline nature of the samples was examined, which was confirmed by XRD, FTIR, and EDAX analysis. The composites were prepared using melamine-derived g-C₃N₄ using a simple ultrasonication technique. 3, 5, 10, and 30 wt% Fe₃O₄ nanoparticles were incorporated in the g-C₃N₄ matrix, and their Fenton, photo, and photo-Fenton processes were studied using rhodamine dye. The 5 wt% composite showed superior performance with 98% degradation efficiency within 30 minutes. It also showed a 1.24 and 2.15-fold increase in the rate constant when compared to pure Fe₂O₃ and g-C₃N₄ samples, respectively. Their super-paramagnetic properties help in the easy separation of the catalyst after the reaction. The catalyst also has at least five times the re-usability in the photo-Fenton process. These results may help us understand and develop iron-based heterogeneous systems for advanced oxidation processes.

KeyWords: Fenton process, Fe₃O₄/g-C₃N₄ nanocomposites, Photo-degradation, Rhodamine dye.

^{1,2*,3,4,5,6}Center for Nanoscience and Technology, K.S. Rangasamy College of Technology, Tiruchengode 637 215, Namakkal (Dt.), Tamil Nadu, India

***Corresponding Author:** satheeskumars@ksrct.ac.in

*Center for Nanoscience and Technology, K.S. Rangasamy College of Technology, Tiruchengode 637 215, Namakkal (Dt.), Tamil Nadu, India

DOI: 10.48047/ecb/2023.12.si5a.0220

INTRODUCTION

Rapid technological advancement and excessive consumption of raw materials have put a lot of strain on our ecology in recent years. There is an urgent need to address major environmental challenges. Although the Fenton process is a promising industrial wastewater treatment method, its principal drawbacks are its relatively high cost and the significant amount of ferric sludge it generates when neutralizing the treated solution before disposal. The photo-Fenton technique, which improves OH radical production, can overcome these limitations. Heterogeneous Fenton reactions are also now being studied due to their advantage of reusing Fenton sludge. Due to its basic operation, straightforward experimental setup, and superior water pollution degradation impact, the heterogeneous photo-Fenton is recognized as an efficient contamination removal technique^[1-6].

In most cases, the photo-generated electrons on the catalyst surface brought on by light irradiation will convert iron(III) to iron(II), thereby assisting in the production of more OH radicals in the reaction system. Thus, it is necessary to create, research, and develop various photo-Fenton catalytic systems^[7-9]. Fe₃O₄ has drawn particular interest in the field of photo-Fenton for emerging contaminants in water effluents because to its greater structural Fe²⁺ content, low cost, strong environmental protection, and interesting magnetic characteristics^[10,11]. Recently, Zanchettin et al. demonstrated that the Fe₃O₄ nanoparticles exhibit outstanding photo-Fenton activity for the tetracycline and reactive azo dye MO degradation under visible light^[12]. However, a disadvantage of the magnetic nanoparticle aggregation is that Fe₃O₄'s surface area is reduced, this can be addressed by building nanocomposites based systems^[13,14].

The quick microwave-assisted solvothermal approach is still a barrier to the scale-up production of these Fe₃O₄ nanoparticles^[15,16], hence a straightforward sol-gel method is used in this instance to create gram-scale nanoparticles, also we have used Fe²⁺ as a single iron ion source for the preparation of Fe₃O₄ nanoparticles, which is possible due to oxidation of Fe²⁺ in basic medium upon certain conditions^[17,18].

Due to its high removal efficacy in degrading and mineralizing organic contaminants from water, photocatalysis methods have attracted increased interest in the field of water treatment^[19-21]. Moreover, photocatalysis techniques are more

environmentally benign than other treatment methods like physical and chemical ones since they do not emit harmful residues or change organic contaminants^[22-25]. To be more precise, during the photocatalysis, a range of organic pollutants would be destroyed or mineralized into intermediate products of CO₂ and H₂O^[26,27].

The graphitic carbon nitride (g-C₃N₄) is a nonmetallic semiconductor with a bandgap of 2.7 eV that offers good UV and visible light absorption. It just contains Carbon and Nitrogen. The g-C₃N₄ is stable, resistant to acids, alkalis, and light-induced disintegration, and its structure can be modified to have certain qualities^[28-31]. In terms of photo-catalyst formulations, g-C₃N₄ research is currently at the forefront. The use of g-C₃N₄ is nevertheless constrained by the quick electron-hole recombination and the low photocatalytic efficiency of photo-generated electrons^[32,33].

As previously mentioned, this issue can be resolved using a range of modification techniques, such as doping g-C₃N₄ with metal or non-metal elements to adjust its bandgap and stop electrons and holes from recombining^[34-37]. The efficiency of the separation of the electrons and holes in g-C₃N₄ has been increased through doping, noble metal modification, and combinations with other semiconductors. Synergistic effects allowed Lei et al. to create composites of g-C₃N₄ and Bi₂WO₆, which considerably improved their photocatalytic performance^[38]. The presence of WO₃ with g-C₃N₄ is advantageous for electron transport and significantly raises the composites' photocatalytic efficiency^[39]. The modification of MoS₂ nanosheets on g-C₃N₄ might add more active sites and increase the effectiveness of its photodegradation^[40].

Recently, Magnetically Separable Mesoporous Fe₃O₄/g-C₃N₄ as a multifunctional material for metallic ion adsorption, oil removal from the aqueous phase, Photo catalysis, and efficient synergistic photo activated Fenton Reaction^[41]. This motivated to study Fe₃O₄/g-C₃N₄ for degradation of organic pollutants^[42-49]. In this research, simple surfactant free sol-gel synthesis of Fe₃O₄ is prepared and melamine derived g-C₃N₄ are prepared following solution processed composite preparation.

MATERIALS AND METHODS

Ferrous sulfate heptahydrate (FeSO₄·7H₂O, ≥98%), Sodium hydroxide (NaOH, ≥98%), hydrochloric acid (HCl, 36.0–38.0%), Rhodamine

B (RhB), Hydrogen peroxide (H₂O₂, 30%), Melamine (98%), ethanol (99%) were purchased from Nice chemical, Kerala, India. All chemicals were of laboratory grade and used as received. All the chemicals were used directly without any further purification. Double distilled water was used throughout the experiment.

SYNTHESIS

g-C₃N₄ Synthesis

Graphitic carbon nitride is made by thermal polymeric condensation of melamine. To do this, 10 grams of melamine are loaded into a 100 ml dry porcelain crucible and covered with a lid. The crucible is then placed in a muffle furnace and slowly heated to 550°C over the course of 30 minutes, where it is maintained for two hours. The furnace is then extinguished, allowed to cool over night, and the sample is extracted the next day. The solid piece of lemon yellow is placed in a mortar, ground to a fine powder, and labeled as CN.

Fe₃O₄ Synthesis

Fe₃O₄ nanoparticles are prepared by simple sol-gel method using single salt precursor. 100ml of DD water is taken in a beaker and stirred for 10 minutes at room temperature using magnetic stirrer and hot plate setup. Then 4.17 gram of ferrous sulphate heptahydrate is dissolved in 20 ml DD water using a bath sonicator and mixed to the above solution. The solution is heated using hot plate and 30 grams sodium hydroxide is slowly added after 30 minutes upon heating up to 80°C, the pale green ferrous sulphate solution turns light brown upon addition of NaOH and slowly turns to form dark brown precipitate. The solution is removed, cooled to room temperature and magnets are used for separation of precipitate and washed several times using double distilled water. The final precipitate is re-dispersed in ethanol and precipitate is extracted and dried over night in hot air oven at 60°C. The sample is scrapped and labeled as FO.

Composite preparation

Fe₃O₄/g-C₃N₄ composite is prepared by simple solution dispersion technique. 250 mg of FO is taken for the 50Wt% with 25 ml of DD water and sonicated for 15 min. Then, another 250 mg of CN is dispersed in 25 ml of DD water in separately. After that the above two solution is mixed and sonicate for 15 min. Following centrifugation and drying, the samples and grey colour power is obtained. The dried sample is named as CN5FO. The same treatment is applied for various wt%

samples labeled as CN5FO, CN10FO, and CN30FO.

Photo-Fenton Degradation process

In this method rhodamine-B dye solutions were taken 50 ml concentration of 100 ppm added with 50 mg of prepared nanocomposites. The pH is maintained at 2 by adding 1M HCl and 0.03 ml H₂O₂ is added to the mixture. Before exposing the solution is kept in dark for 15 minutes to attain adsorption-desorption equilibrium.

Then the above solution was exposed to full sun irradiation by placing directly at mid day on a sunny day. After that every 10 mins 2mL of solution is extracted. After centrifuging the 1ml top aliquot is extracted and absorption intensity was analyzed at 357 nm using visible spectrophotometer. The degradation curve was obtained and estimated photo-Fenton degradation efficiency. For Fenton process the same reaction conditions are maintained without sun irradiation. In photo degradation studies the performance are estimated using the prepared samples against Rhodamine-B with sun irradiation.

The catalytic stability of the composite was studied utilizing a cycling experiment. Absolute ethanol and distilled water were used to wash the composite until the pH of the solution was neutral. The composite was then dried in a hot air oven for 24 hours at 60 °C. The separated catalyst was used for recycle.

Characterization

The crystal structure of the prepared samples was analyzed using powder X-ray diffractometer, bruker D8-Advance X-ray diffraction (XRD). Fourier transform infrared spectroscopy (FT-IR) was used to understand the organic bonds present in the sample thermo fisher Nicolet iS50 spectrometer was used with the measuring range of 4000 - 500 cm⁻¹. The surface and morphology studies where performed using FESEM with EDS analysis,(SIGMA HV – Carl Zeiss With Bruker Quantax 200 – Z10 EDS Detector) and High Resolution Transmission Electron Microscopy HRTEM (JEOL JEM 2100)The thin film UV-Vis absorption spectrum of samples are analyzed using SHIMADZU, UV 3600 PLUS. The magnetic properties were measured by Lake shore vibrating sample magnetometer (VSM). Impedance analysis was done using AUTOLAB Netherlands electrochemical workstation.

Results and discussion

XRD Analysis

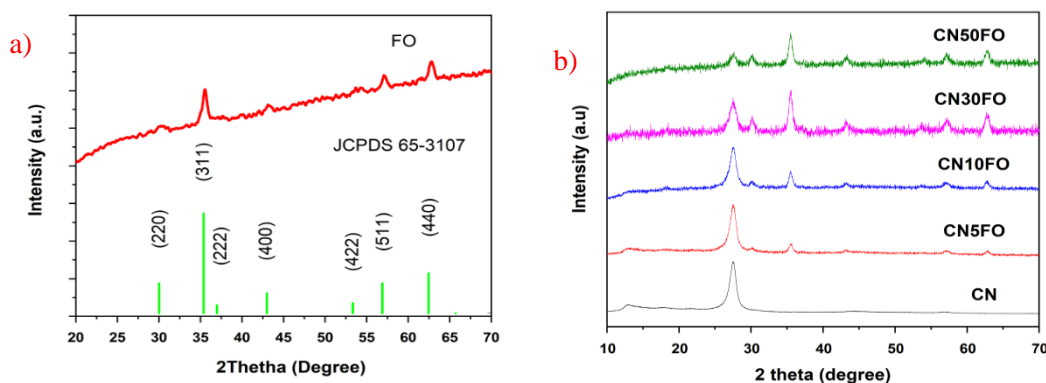


Figure 1 (a) & (b) shows the XRD diffraction of prepared samples

Fig. 1(a) and (b) shows that XRD diffraction of samples prepared nanocomposites. Figure 1(a) showed all diffraction peaks of FO sample that can be indexed to a pure, crystalline, face-centered cubic spinel structure of Fe_3O_4 ^[11]. The diffraction peaks of (220), (311), (400), (440), (422), (511), and (440) could be observed at the 2θ degree value of 30.2° , 35.6° , 43.3° , 53.5° , 57.1° , and 62.7° respectively, which are in accordance with the standard Fe_3O_4 crystal data (JCPDS Card No. 65-3107). No further unwanted peaks were seen in the sample which shows us that there were no other impurities and phase impurities in the sample. Fig 1(b), pure $g-C_3N_4$ shows a prominent peak at 27.5° that corresponds to the (002) plane and a small peak at 13° that corresponds to (100) plane which are attributed to the in-plane structural packing motif and interlayer stacking of the aromatic structures of graphitic carbon nitride, respectively.

The composite samples showed both the peaks of Fe_3O_4 and $g-C_3N_4$ planes with no other peak showing good purity of composites prepared. Also the peak intensity of Fe_3O_4 showed gradually increase with increased in weight percentage of FO

nanoparticles. No peak shift is observed in $g-C_3N_4$ peaks showing there was no structural change of graphitic layers of carbon nitride. The nanoparticles would have adhered on the $g-C_3N_4$ material without disturbing its lattices^[42].

UV-Vis analysis

The light absorption properties of the as-prepared samples were measured by UV-Vis. spectrometer. The UV-Vis. spectra of FO, CN, CN5FO, CN10FO, CN30FO and CN50FO were acquired and are shown in Fig. 2(a). The CN spectrum shows the characteristic peaks of $g-C_3N_4$ nature^[41]. The light absorption edge of pure $g-C_3N_4$ is about 330 nm. The pure FO exhibited profound absorption over a wide range of spectra from UV to visible light with strong absorption in UV region. After the introduction of FO into CN, the composite samples exhibited enhanced optical absorption in the visible region around 400 nm compared with CN, and the absorption intensities of these composites are strengthened with increase in the FO content in the sample. It is well known that enhancing absorption in the visible light region improves the activity of a photo-catalyst.

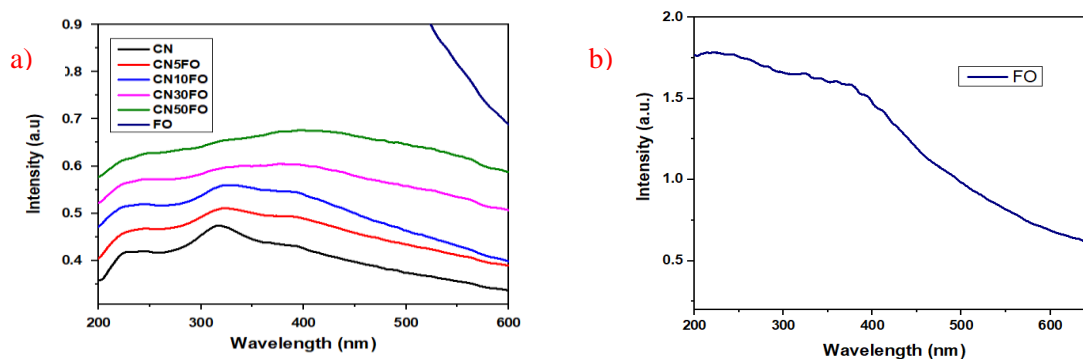


Figure 1 (a), (b) UV-Vis spectrum of prepared samples

The band gap is estimated using tauc plot. The FO showed the band gap energy of 1.95 eV, while CN showed the band gap of 2.74 eV which agreed with the previously reported band gap energy^[48] while the composite showed decrease in band gap when compared to CN. The CN5FO, samples showed the band gap energy as 2.34, eV which is suitable for photocatalysis.

These results indicate that the g-C₃N₄-Fe₃O₄ composite absorption edge shifted to a longer wavelength and the ability to absorb visible light improved as the Fe₃O₄ to g-C₃N₄ weight ratio increased. The increase in visible light absorption may have been caused by heterogeneous structures forming and also with volume of FO added to the sample. The results imply that absorption shift of the photocatalyst to visible light may be improved by loading Fe₃O₄ onto the g-C₃N₄ sheets.

PL analysis

The PL spectra of photo catalysts is shown in fig. 3 (a) which can be used to illustrate the recombination rate of the photo generated electron-hole pairs, it could be known that the higher PL intensity usually means more recombination of

electron-hole pairs and lower photocatalytic activity. The below figure shows the PL spectra of the as-prepared samples of FO, CN, CN5FO, CN10FO, CN30FO and CN50FO. All of the photo catalyst exhibited a broad emission peak centered about 490 nm which could be due to the Band photo luminescence phenomena of the excited charge carriers in g-C₃N₄ matrix. It can be observed that, the CN have a strong PL peak under an excitation wavelength of 440 nm which is the characteristic PL emission of g-C₃N₄, which could be related to the recombination of the photogenerated electron-hole pairs in g-C₃N₄. In composites, the emission peak intensities significantly decreased, indicating that the recombination of electron-hole pairs is greatly suppressed by the introduction of FO. One reason might be that coupling which may change the transition path of photogenerated electrons to the ground state for CN. As a result, the charge separation could be promoted on the composites, leading to the higher photocatalytic activity in the composites. The luminous intensity of composites was between CN and FO, indicating that FO and CN have a synergistic effect and are favorable for the enhancement of photo-catalytic performance.

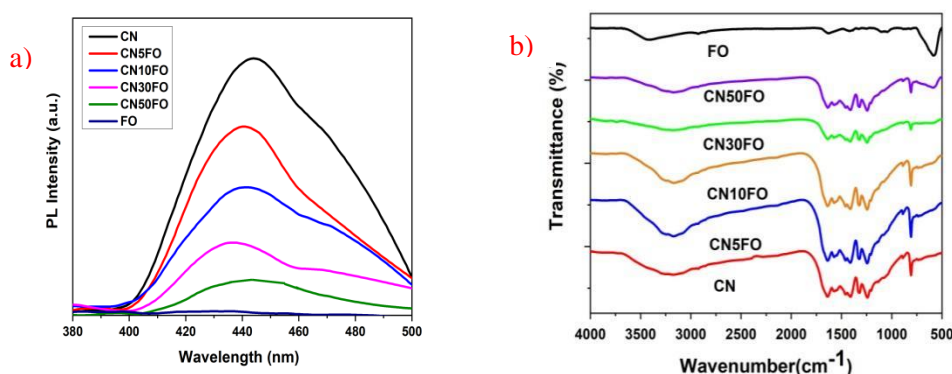


Figure 3 (a), PL emission (b) FTIR spectrum of samples prepared

FTIR analysis

The FTIR analysis is shown in fig 3(b). In the FTIR spectrum of CN, a series of bands, the sharp peaks at 805 cm⁻¹, 1246–1638 cm⁻¹, are attributed to respiration modes of the triazine units of g-C₃N₄. The characteristic band at 1246 cm⁻¹ and 1638 cm⁻¹ can be attributed to tensile vibration of the -CN heterocyclic ring. The peak at 3000–3600 cm⁻¹ is the tensile vibration absorption peak of NH bond. While the broad band at 3000-3500 cm⁻¹ is ascribed to stretching vibration of N-H groups and surface adsorbed -OH groups. In addition, the band at 810

cm⁻¹ originates from a breathing mode of s-triazine characteristic. When different amounts of FO are added into g-C₃N₄, the peak position does not shift; however, the intensity values are reduced. In the spectrum of FO, the strong characteristic peak at 580 cm⁻¹ is due to vibrations of Fe-O bond. However, we could not observe any bands correspond to Fe-N and Fe-C bond vibrations in CN-FO composites, the FTIR spectra of CN-FO composites are similar to that of pure CN, and all the characteristic absorption bands of CN appear in the composites. Also, Fe-O absorption band was

prominent upon increase in FO content in the composites, suggesting that no structure change of CN appears during the composite preparation. This

showed that the incorporation of FO, the skeleton structure of $g-C_3N_4$ does not vary.

FESEM and EDAX Analysis:

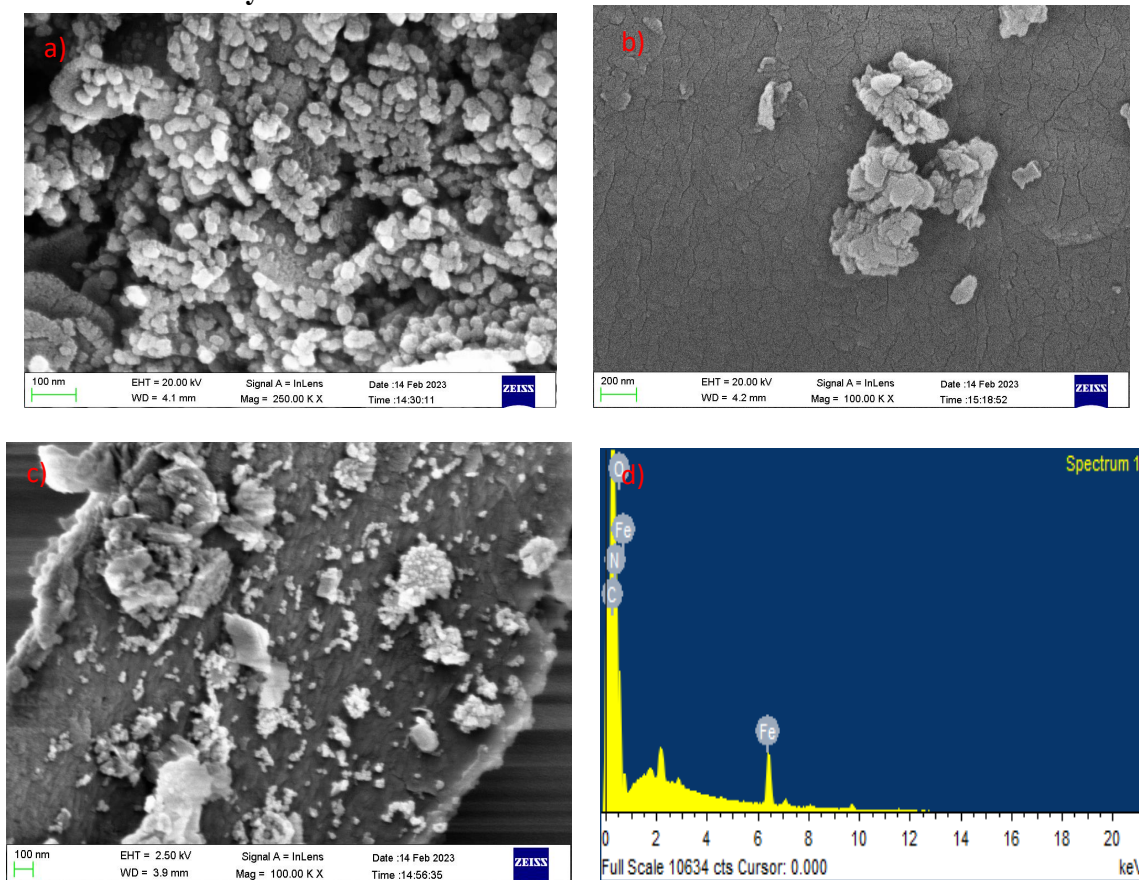


Figure 4 (a-c) shows the FESEM images of CN, FO and CN5FO samples. (d) EDAX of CN5FO samples

The fig. 4(a-c) shows the FESEM images of FO, CN and CN5FO samples. The FO sample showed fine particles that are agglomerated throughout the sample. They were in the range of 20 to 50 nm and no other morphology or bulk particles were found in the sample showing that our material produced uniformly structured iron oxide nanoparticles. The particles were poly dispersed in nature. The CN sample showed flake like morphology that are packed together and had smooth surface. These are

the characteristic morphology of bulk graphitic carbon nitride. The composite showed the presence of both $g-C_3N_4$ and Fe_2O_3 nanoparticles.

The nanoparticle was well dispersed on to $g-C_3N_4$ material. Although few agglomerated Fe_3O_4 nanoparticles are seen in the sample. This shows that the composite has well dispersed iron oxide nanoparticles into the $g-C_3N_4$ structures.

HRTEM Analysis

a)

b)

c)

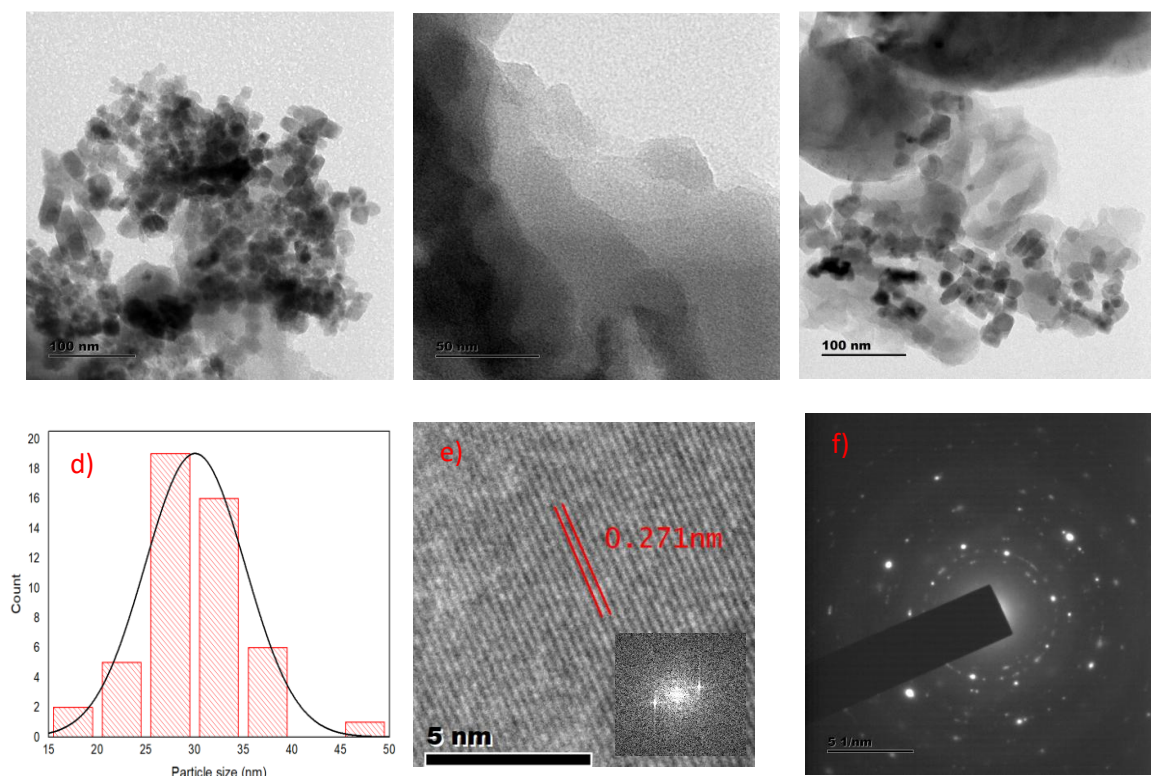


Figure 5 TEM images of (a) FO, (b) CN, (c) CN5FO. (d) Histogram of FO particles, (e) HRTEM image of FO crystal, inner image shows the FFT of the same., (f) SAED pattern of FO.

The fig 5 (a-b) shows the TEM analysis of FO, CN and CN5FO samples. The FO samples shows particles that are fine in nature with the size range of 20-50nm. The histogram (fig. 5(d)) shows the average particle diameter to be 30nm. The particles where polycrystalline in nature which was revealed by the SAED pattern (fig. 5(f)) for the same. The HRTEM images (fig. 5(e)) of the particles showed crystalline arrangement of atoms.

The FFT image of these HRTEM images showed the crystalline nature and revealed diffraction pattern and the d spacing value was found to be 0.271nm which corresponds to the (311) plane. The sample showed agglomerated iron oxide nanoparticles throughout the analysis. There was no other bulk or differently sized materials showing that the sample consists of only iron oxide nanoparticles. The nanoparticles had sharp edged which shows us that it may form into cubical structures upon further optimization of synthesis protocol. The $g-C_3N_4$ sample showed the layered morphology of $g-C_3N_4$ with smooth surface. The graphite like morphology was very evident in the sample with no other morphology. The CN5FO sample showed that the iron oxide nanoparticles where well dispersed on to the layered morphology of $g-C_3N_4$ structures. There were no major

agglomeration of nanoparticles sample on $g-C_3N_4$ showing that the nanoparticles are well dispersed throughout the sample.

Degradation studies

The Fenton, photo and photo-Fenton photocatalytic activities of CN, FO and CN-FO composites were determined using the catalytic degradation of Rhodamine B dye when exposed to solar light (peak sun time 11-2 pm where chosen). The fig 6 shows the photocatalytic activity of all samples as Fenton, photo and photo Fenton processes. For Fenton studies the catalyst is added with the organic dye solution at acidic pH in presence of hydrogen peroxide and kept in a dark atmosphere throughout the studies. The Fenton reaction was very slow for all the samples. FO pure sample showed better performance than all the samples. This is expected as we know the amount of iron ions plays crucially for the Fenton process to occur. More the Fe_3O_4 nanoparticles in the catalyst faster were the Fenton process. Anyway CN showed no noticeable degradation of sample even up to 1000 min of the reaction time. This very well corresponds to the theory that presence of iron atoms or ions are crucial for the Fenton process to occur.

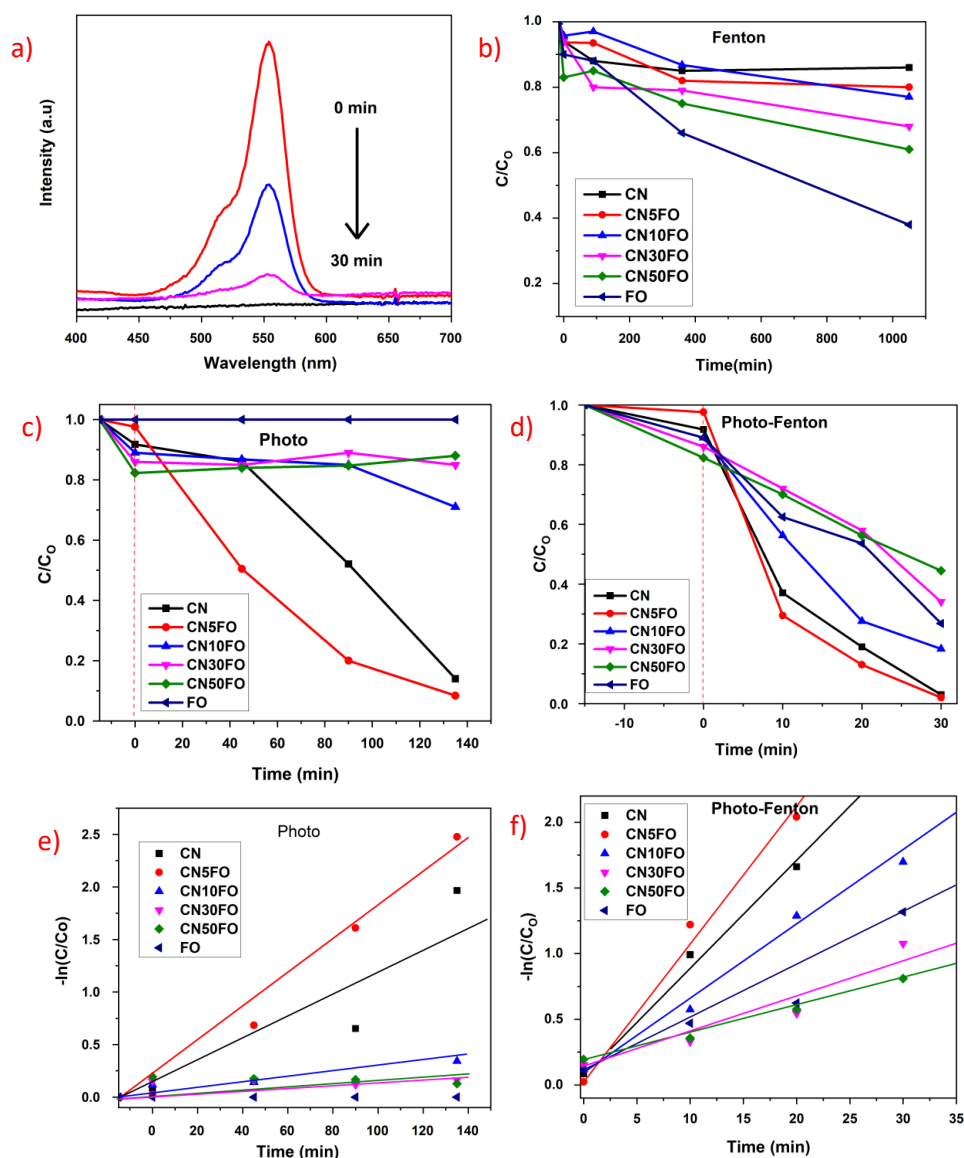


Figure 6 UV-Vis absorption spectra of RhB dye during the photo-Fenton reaction using CN5FO. (b), (c) and (d) Fenton, photo and photo-Fenton degradation of RhB dye using various catalyst prepared. (e), (f) logarithmic graph of photo and photo-Fenton process.

Anyway maximum decomposition of C/C_0 value decreasing up to 0.35 was seen in FO sample at 1000 mins. Anyway this performance is very slow and may not have day to day usage. Next the photo catalytic activity is seen by simply adding the catalyst to RhB solution upon exposure to solar irradiation. The photo catalytic activities of the composites were closely related to the compositions of the composites. In this case, the pure FO sample showed least performance, no significant change in dye concentration seen upto 140 mins. The 5 wt% FO in $g-C_3N_4$ sample showed superior performance when compared to pure CN which being the second best sample to performance and anything above 5 wt% addition of FO showed less degradation properties proportional to the amount of FO added in the sample. The Photo Fenton process is carried out by exposing the

Eur. Chem. Bull. **2023**, *12*(Special Issue 5), 3322 – 3333

freshly prepared Fenton process samples to solar irradiation. The similar catalytic performance trend is seen to the photo catalytic studies but the time period to achieve the same degradation was greatly decreased for all samples. The 5 wt% FO in CN composite showed outstanding performance of 96% degradation rate at 30 minutes time. The CN sample showed second best results. And addition of anything more than 5 wt% FO showed decrease in photon Fenton catalytic performances. The enhanced photo-catalytic activities of the 5wt% composite could have been caused by the composites having higher surface areas, higher visible-light absorption capacities, and higher electron-hole separation efficiencies.

The data acquired using visible spectrometer were used to analyse the degradation kinetic of RhB dye

3329

and it was found that a pseudo-first order model fitted with the data. The formula for the pseudofirst-order model is

$$\ln(C_0/C) = kt,$$

where C₀ is the initial concentration of RhB Dye (100mg/l) in the aqueous solution, c is the actual concentration of the dye at the specified time during the reaction, k is the degradation rate constant, and t is the reaction time^[45]

The rate constants k and Degradation efficiency for the different samples are shown in Fig. 7 (a). It is worth noting that the photocatalytic activities of the composite increased when 5 wt% FO was added to CN while further increase in FO only resulted in reducing of the performance of the catalyst. The CN5FO showed the highest rate constant, 0.0861

min⁻¹, which was almost 1.25 times higher than the rate constant for pure CN sample and 2.14 times higher than pure FO sample. This may have been because combining a small portion of Fe₃O₄ nanoparticles to g-C₃N₄ could allow hetero junction to form, giving the composite a lower rate of electron-hole pair recombination. This would have meant that more h⁺ and e⁻ would have been generated to participate in the degradation process, enhancing the photocatalytic activity. However, increasing the amount of Fe₃O₄ present further would have allowed some Fe₃O₄ to act as a recombination center for photo-induced electrons and holes, and may have caused the active sites on the g-C₃N₄ surfaces to be covered, decreasing the photocatalytic activity of the composite. It is therefore very important that the most appropriate degree of doping is achieved to improve photocatalytic activity.

EIS, CYCLE AND VSM Studies

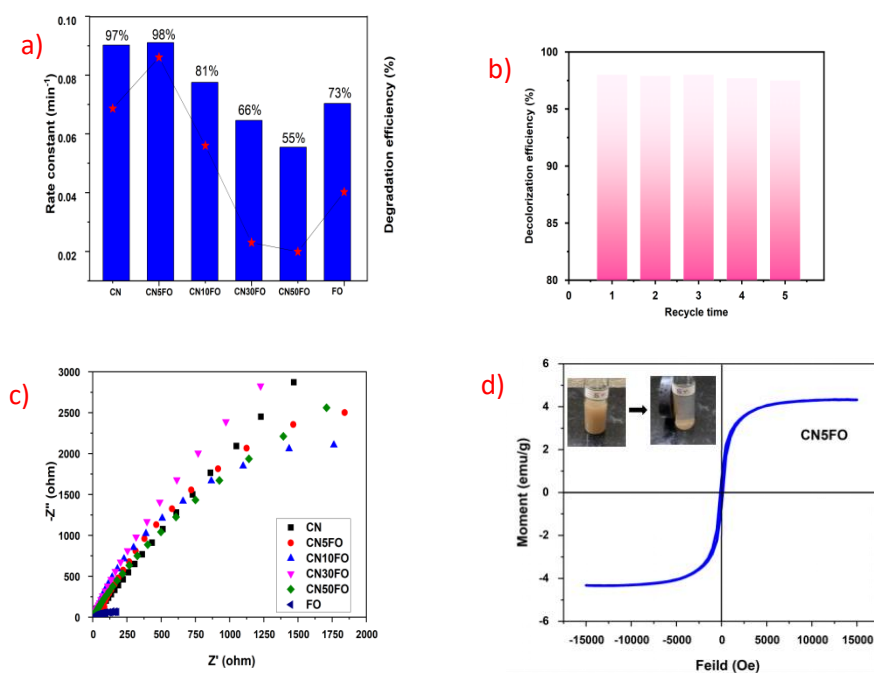


Figure 7(a) rate constant and degradation efficiency chart, (c) Nyquist plot of composites 7(a) rate constant and degradation efficiency chart, (c) Nyquist plot of composites prepared. (b) cycle graph and (d) VSM of CN5FO.

The electro-chemical impedance studies were conducted for all our prepared samples. The figure 7(c) showed the Nyquist plot of the sample with a linear fit. The lower weight percentage iron oxide nanoparticles showed smaller arc radius when compared to pure g-C₃N₄. The smaller Nyquist arc radius indicated faster charge transfer and lower charge-transfer resistance of the sample, which can be attributed to the better performance of our composite sample in photo-Fenton degradation process when compared to pure samples prepared.

The CN5FO samples were recycled 5 times and their performance was recorded at 30 minutes in photo-Fenton degradation of RhB dye. The catalyst performed throughout the five cycles a slight dip in performance from fourth cycle was observed being 97% efficiency. This shows that the prepared nanocomposite can be recycled multiple times without any noticeable drop in degradation efficiency.

The fig 7 (d) displays the VSM curve taken at ambient temperature of CN5FO nanocomposite with the inner image showing a colour photograph of composite suspension in water without and with external magnetic field. Due to the presence of Fe₃O₄ nanoparticles in our composite they showed no hysteresis remanence or coercivity, which indicated that they had the representative super paramagnetic property which is well known property of magnetic nanoparticles. Saturation magnetization of the CN5FO was 4.3 emu/g, and they displayed super paramagnetic behavior. By placing an external magnet beside the glass bottle containing the CN5FO nanocomposite, the particles were readily attracted to the wall of the glass bottle within 10 minutes, as shown in the top-left inset of Fig, suggesting an easy separation under external magnetic field which is an important advantage for separation of photo-catalyst from treated water.

CONCLUSION

Fe₃O₄ nanoparticles were prepared by simple sol-gel surfactant free method using single ion precursor, with an average particle size of 30 nm, they showed polycrystalline nature with good elemental and crystalline purity. These nanoparticles are added with melamine derived g-C₃N₄ to form photo catalyst. The 5 wt% of Fe₃O₄ nanoparticles showed superior photo-Fenton degradation of RhB dye when compared to pure samples. The CN5FO showed 98% degradation efficiency within 30 minutes time. It also showed 1.24 and 2.15 times increase in rate constant when compared to pure FO and CN samples. The composite was super-paramagnetic in nature making it easily separable from dye solution. The catalyst also showed good re-usability in nature, which may be a promising candidate to treat organic waste water.

REFERENCES

1. X. Liu, J. Iocozzia, Y. Wang, X. Cui, Y. Chen, S. Zhao, Z. Li, Z. Lin, Noble metal-metal oxide nanohybrids with tailored nanostructures for efficient solar energy conversion, photocatalysis and environmental remediation, *Energy Environ. Sci.* 10 (2017) 402-434.
2. Crini, G., and Lichtfouse, E. "Advantages and disadvantages of techniques used for wastewater treatment," *Environmental Chemistry Letters*, V. 17, No. 1, 2018, pp. 145-55.
3. FN, C., and MF, M. "Factors Affecting Water Pollution: A Review," *Journal of Ecosystem & Ecography*, V. 07, No. 01, 2017.
4. Savitha, S., Surendhiran, S., Jagan, K. S. G., Karthik, A., Kalpana, B., Senthilmurugan, R. "Evaluation of the physicochemical characteristics and photocatalytic activity of cobalt oxide nanoparticles derived from Moringa seed extract," *Journal of Materials Science: Materials in Electronics*, V. 34(2), 2023, p. 1-19.
5. Jagan, K. S. G., Surendhiran, S., Savitha, S., Balu, K. S., Karthick, M., Vidaarth, T. N., Senthilmurugan, R. "Influence of different alkaline actuators in the synthesis of NiO NPs: A comparative green approach on photocatalytic and in vitro biological activity," *Inorganic Chemistry Communications*, v. 151, 2023, p. 110618.
6. Anithadevi, R., Ravichandran, C., "Enhanced photo-degradation activity of hybrid ZnMgTiO₂ nanocomposites against methyl orange dye under uv irradiation," v. 14, Nr. 6, 2018, p. 449-457.
7. Xu, M., Wu, C., and Zhou, Y. "Advancements in the Fenton Process for Wastewater Treatment," *Advanced Oxidation Processes - Applications, Trends, and Prospects*, 2020.
8. Zhang, M., Dong, H., Zhao, L., et al. "A review on Fenton process for organic wastewater treatment based on optimization perspective," *Science of The Total Environment*, V. 670, 2019, pp. 110-21.
9. Pliego, G., Zazo, J. A., Garcia-Muñoz, P., et al. "Trends in the Intensification of the Fenton Process for Wastewater Treatment: An Overview," *Critical Reviews in Environmental Science and Technology*, V. 45, No. 24, 2015, pp. 2611-92.
10. Wei, Y., Han, B., Hu, X., et al. "Synthesis of Fe₃O₄ Nanoparticles and their Magnetic Properties," *Procedia Engineering*, V. 27, 2012, pp. 632-7.
11. Zheng, Y., Cheng, Y., Bao, F., et al. "Synthesis and magnetic properties of Fe₃O₄ nanoparticles," *Materials Research Bulletin*, V. 41, No. 3, 2006, pp. 525-9.
12. Boruah, P. K., Sharma, B., Karbhal, I., et al. "Ammonia-modified graphene sheets decorated with magnetic Fe₃O₄ nanoparticles for the photocatalytic and photo-Fenton degradation of phenolic compounds under sunlight irradiation," *Journal of Hazardous Materials*, V. 325, 2017, pp. 90-100.
13. Yang, X., Chen, W., Huang, J., et al. "Rapid degradation of methylene blue in a novel heterogeneous Fe₃O₄@rGO@TiO₂-catalyzed photo-Fenton system," *Scientific Reports*, V. 5, No. 1, 2015.

14. Zanchettin, G., Falk, G. da S., González, S. Y. G., et al. "High performance magnetically recoverable Fe₃O₄ nanocatalysts: fast microwave synthesis and photo-fenton catalysis under visible-light," *Chemical Engineering and Processing - Process Intensification*, V. 166, 2021, p. 108438.
15. Yu, L., Chen, J., Liang, Z., et al. "Degradation of phenol using Fe₃O₄-GO nanocomposite as a heterogeneous photo-Fenton catalyst," *Separation and Purification Technology*, V. 171, 2016, pp. 80–7.
16. Arshad, A., Iqbal, J., Ahmad, I., et al. "Graphene/Fe₃O₄ nanocomposite: Interplay between photo-Fenton type reaction, and carbon purity for the removal of methyl orange," *Ceramics International*, V. 44, No. 3, 2018, pp. 2643–8.
17. Wang, G., Bowden, M. E., Saslow, S. A., et al. "Micrometer-sized magnetite synthesis using Fe(OH)₂(s) as a precursor for technetium sequestration from liquid nuclear waste streams," *Journal of Nuclear Materials*, V. 552, 2021, p. 152964.
18. A., et al. "Transformation mechanism of magnetite nanoparticles," *Materials Science-Poland*, V. 33, No. 2, 2015, pp. 278–85.
19. Karunakaran, C., Vinayagamorthy, P., and Jayabharathi, J. "Nonquenching of Charge Carriers by Fe₃O₄ Core in Fe₃O₄/ZnO Nanosheet Photocatalyst," *Langmuir*, V. 30, No. 49, 2014, pp. 15031–9.
20. Zhai, Y., Yin, Y., Liu, X., et al. "Novel Magnetically Separable BiVO₄/Fe₃O₄ Photocatalyst: Synthesis and Photocatalytic Performance under Visible-light Irradiation," *Materials Research Bulletin*, V. 89, 2017, pp. 297–306.
21. Liu, H., Jia, Z., Ji, S., et al. "Synthesis of TiO₂/SiO₂@Fe₃O₄ magnetic microspheres and their properties of photocatalytic degradation dyestuff," *Catalysis Today*, V. 175, No. 1, 2011, pp. 293–8.
22. Maeda, K., Teramura, K., Lu, D., et al. "Photocatalyst releasing hydrogen from water," *Nature*, V. 440, No. 7082, 2006, pp. 295–295.
23. Kudo, A., and Miseki, Y. "Heterogeneous photocatalyst materials for water splitting," *Chem. Soc. Rev.*, V. 38, No. 1, 2009, pp. 253–78.
24. Lee, S.-Y., and Park, S.-J. "TiO₂ photocatalyst for water treatment applications," *Journal of Industrial and Engineering Chemistry*, V. 19, No. 6, 2013, pp. 1761–9.
25. Kudo, A. "Development of photocatalyst materials for water splitting," *International Journal of Hydrogen Energy*, V. 31, No. 2, 2006, pp. 197–202.
26. Zhang, H., Lv, X., Li, Y., et al. "P25-Graphene Composite as a High Performance Photocatalyst," *ACS Nano*, V. 4, No. 1, 2009, pp. 380–6.
27. Primo, A., Corma, A., and García, H. "Titania supported gold nanoparticles as photocatalyst," *Phys. Chem. Chem. Phys.*, V. 13, No. 3, 2011, pp. 886–910.
28. Wen, J., Xie, J., Chen, X., et al. "A review on g-C₃N₄ -based photocatalysts," *Applied Surface Science*, V. 391, 2017, pp. 72–123.
29. Fu, J., Yu, J., Jiang, C., et al. "g-C₃N₄-Based Heterostructured Photocatalysts," *Advanced Energy Materials*, V. 8, No. 3, 2017, p. 1701503.
30. Zhu, B., Cheng, B., Fan, J., et al. "g-C₃N₄-Based 2D/2D Composite Heterojunction Photocatalyst," *Small Structures*, V. 2, No. 12, 2021, p. 2100086.
31. Zhao, Y., Shi, H., Yang, D., et al. "Fabrication of a Sb₂MoO₆/g-C₃N₄ Photocatalyst for Enhanced RhB Degradation and H₂ Generation," *The Journal of Physical Chemistry C*, V. 124, No. 25, 2020, pp. 13771–8.
32. Bai, X., Wang, L., Wang, Y., et al. "Enhanced oxidation ability of g-C₃N₄ photocatalyst via C60 modification," *Applied Catalysis B: Environmental*, V. 152–153, 2014, pp. 262–70.
33. Liu, X., Ma, R., Zhuang, L., et al. "Recent developments of doped g-C₃N₄ photocatalysts for the degradation of organic pollutants," *Critical Reviews in Environmental Science and Technology*, V. 51, No. 8, 2020, pp. 751–90.
34. Yuan, Y.-J., Shen, Z., Wu, S., et al. "Liquid exfoliation of g-C₃N₄ nanosheets to construct 2D-2D MoS₂/g-C₃N₄ photocatalyst for enhanced photocatalytic H₂ production activity," *Applied Catalysis B: Environmental*, V. 246, 2019, pp. 120–8.
35. Mamba, G., and Mishra, A. K. "Graphitic carbon nitride (g-C₃N₄) nanocomposites: A new and exciting generation of visible light driven photocatalysts for environmental pollution remediation," *Applied Catalysis B: Environmental*, V. 198, 2016, pp. 347–77.
36. Ngullie, R. C., Alaswad, S. O., Bhuvaneshwari, K., et al. "Synthesis and Characterization of Efficient ZnO/g-C₃N₄ Nanocomposites Photocatalyst for Photocatalytic Degradation of Methylene Blue," *Coatings*, V. 10, No. 5, 2020, p. 500.
37. Shi, W., Wang, J., Yang, S., et al. "Fabrication of a ternary carbon dots/CoO/g-C₃N₄ nanocomposite photocatalyst with enhanced

- visible-light-driven photocatalytic hydrogen production,” *Journal of Chemical Technology & Biotechnology*, V. 95, No. 8, 2020, pp. 2129–38.
38. Liu, L., Qi, Y., Lu, J., et al. “Dramatic activity of a Bi₂WO₆@g-C₃N₄ photocatalyst with a core@shell structure,” *RSC Advances*, V. 5, No. 120, 2015, pp. 99339–46.
39. Zhao, J., Ji, Z., Shen, X., et al. “Facile synthesis of WO₃ nanorods/g-C₃N₄ composites with enhanced photocatalytic activity,” *Ceramics International*, V. 41, No. 4, 2015, pp. 5600–6.
40. Tran Huu, H., Thi, M. D. N., Nguyen, V. P., et al. “One-pot synthesis of S-scheme MoS₂/g-C₃N₄ heterojunction as effective visible light photocatalyst,” *Scientific Reports*, V. 11, No. 1, 2021.
41. Mao, H., Zhang, Q., Cheng, F., et al. “Magnetically Separable Mesoporous Fe₃O₄@g-C₃N₄ as a Multifunctional Material for Metallic Ion Adsorption, Oil Removal from the Aqueous Phase, Photocatalysis, and Efficient Synergistic Photoactivated Fenton Reaction,” *Industrial & Engineering Chemistry Research*, V. 61, No. 25, 2022, pp. 8895–907.
42. Zhang, X., Ren, B., Li, X., et al. “High-efficiency removal of tetracycline by carbon-bridge-doped g-C₃N₄/Fe₃O₄ magnetic heterogeneous catalyst through photo-Fenton process,” *Journal of Hazardous Materials*, V. 418, 2021, p. 126333.
43. He, W., Jia, H., Li, Z., et al. “Magnetic recyclable g-C₃N₄/Fe₃O₄@MIL-100(Fe) ternary catalyst for photo-Fenton degradation of ciprofloxacin,” *Journal of Environmental Chemical Engineering*, V. 10, No. 6, 2022, p. 108698.
44. Wang, S., Long, J., Jiang, T., et al. “Magnetic Fe₃O₄/CeO₂/g-C₃N₄ composites with a visible-light response as a high efficiency Fenton photocatalyst to synergistically degrade tetracycline,” *Separation and Purification Technology*, V. 278, 2021, p. 119609.
45. Cui, K.-P., Yang, T.-T., Chen, Y.-H., et al. “Magnetic recyclable heterogeneous catalyst Fe₃O₄/g-C₃N₄ for tetracycline hydrochloride degradation via photo-Fenton process under visible light,” *Environmental Technology*, V. 43, No. 21, 2021, pp. 3341–54.
46. Xu, R., and Peng, Y. “Preparation of Magnetic g-C₃N₄/Fe₃O₄ Composite and Its Application in the Separation of Catechol from Water,” *Materials*, V. 12, No. 18, 2019, p. 2844.
47. Gu, J., Jia, H., Ma, S., et al. “Fe₃O₄-Loaded g-C₃N₄/C-Layered Composite as a Ternary Photocatalyst for Tetracycline Degradation,” *ACS Omega*, V. 5, No. 48, 2020, pp. 30980–8.
48. Xiong, C., Ren, Q., Liu, X., et al. “Fenton activity on RhB degradation of magnetic g-C₃N₄/diatomite/Fe₃O₄ composites,” *Applied Surface Science*, V. 543, 2021, p. 148844.
49. Wang, H., Zhang, C., Zhang, X., et al. “Construction of Fe₃O₄@β-CD/g-C₃N₄ nanocomposite catalyst for degradation of PCBs in wastewater through photodegradation and heterogeneous Fenton oxidation,” *Chemical Engineering Journal*, V. 429, 2022, p. 132445.